X-Ray Refraction Topography and Computed Tomography for NDE of lightweight materials

Bernd R. Müller[*a], Axel Lange[a], Michael Harwardt[a], Manfred P. Hentschel[a],
Bernhard Illerhaus[a], Jürgen Goebbels[a], Joachim Bamberg[b], Falko Heutling[b]
[a]Federal Institute for Materials Research and testing (BAM), Germany;
[b]MTU Aero Engines, Germany

ABSTRACT

X-Ray Refraction Topography techniques are based on Ultra Small Angle Scattering by micro structural elements causing phase related effects like refraction and total reflection at a few minutes of arc as the refractive index of X-rays is nearly unity ($1 \cdot 10^{-5}$). The extraordinary contrast of inner surfaces is far beyond absorption effects. Scanning of specimens results in 2D-imaging of closed and open pore surfaces and crack surface density of ceramics and foams. Crack orientation and fiber/matrix debonding in plastics, polymers and ceramic composites after cyclic loading and hydro thermal aging can be visualized. In most cases the investigated inner surface and interface structures correlate to mechanical properties. For the exploration of Metal Matrix Composites (MMC) and other micro structured materials the refraction technique has been improved to a 3D Synchrotron Refraction Computed Tomography (SR-CT) test station. The specimen is situated in an X-ray beam between two single crystals. Therefore all sample scattering is strongly suppressed and interpreted as additional attenuation. Asymmetric cut second crystals magnify the image up to 50 times revealing nanometer resolution. The refraction contrast is several times higher than "true absorption" and results in images of cracks, pores and fiber debonding separations below the spatial resolution of the detector. The technique is an alternative to other attempts on raising the spatial resolution of CT machines. The given results yield a much better understanding of fatigue failure mechanisms under cyclic loading conditions.

Keywords: Non-Destructive Inspection (NDI), Characterization, Titanium Metal Matrix Composites (Ti-MMC), Ti6242, SCS6.

1   INTRODUCTION

The non-destructive characterization of high performance composites, ceramics and other advanced materials can be difficult. Anisotropy, heterogeneity and complex shapes reduce the performance of traditional non-destructive techniques, which have been optimized for isotropic single phase materials, preferably for metals.

The effect of X-ray refraction provides unconventional small angle X-ray scattering (SAXS) techniques which have been developed and applied in the last decade at our laboratory to meet the actual demand for improved non-destructive characterization of advanced materials. X-ray refraction reveals the inner surface and interface concentrations of nanometer dimensions due to the short X-ray wavelength near 0.1 nm. Sub-micron particle, crack and pore sizes are easily determined by "X-ray refractometry" without destroying the structure by cutting or polishing for microscopic techniques.

Metal Matrix Composites (MMC) are materials based on metal alloys reinforced by ceramic fibers. These composites combine high tensile strength with low specific weight. But there mechanical properties are strongly influenced by the fiber orientation and the interface between the fiber and the matrix as well as the distribution of cracks and pores. While the orientation of the fibers is defined by the production process, the interfaces are also subjected to thermal and mechanical loading of the composite. Since several years titanium based alloy matrices reinforced by SiC fibers (Ti-MMC) are developed in the laboratories of the air and space industry. Used in aircraft engines they can reduce the weight of structural and functional components up to 50 %. The manufacturing technology of Ti-MMC compounds is very challenging but the possibility of non-destructive inspection and characterization of these materials is up to now rather poor. 3D X-Ray Refraction Computed Tomography is a promising tool to reveal the changes and development of the inter surfaces (e.g. fiber-matrix interface, cracks and pores) of those composites.

---

* bernd.Mueller@bam.de: phone +49 30 8104 4635; fax +49 30 8104 3607; www.bam.de/kompetenzen/arbeitsgebiete/abteilung_8/

2   X-RAY REFRACTION

The physics of X-ray refraction is quite similar to the well known refraction of the visible light by optical lenses and prisms, which is governed by Snell's law. However a major difference to the visible optics is, that the refractive index n of X-rays in matter is nearly one[1]. This causes deflections at very small angles in the order of a few minutes of arc.

$$n = 1 - \varepsilon \qquad \text{With} \quad \varepsilon \approx \rho \cdot \lambda^2 \text{ and } \varepsilon \cong 10^{-5} \text{ for glass at 8 keV radiation} \qquad (1)$$

ε is the real part of the complex index of refraction, ρ the electron density and λ the X-ray wavelength. In case of X-rays, where $n < 1$ the converging effect of convex lenses changes to divergence. Fig. 1 demonstrates the effect of small angle scattering by refraction of cylindrical lenses: A bundle of glass fibers with a diameter of 15 μm each as used for glass fibre reinforced plastics (GFRP) deflects collimated parallel X-rays within several minutes of arc. In fibers and spherical particles the deflection of X-rays occurs twice, when entering and when leaving the object (see magnification in Fig. 1). The oriented intensity distribution is collected by an X-ray film or a CCD camera while the straight (primary) beam is omitted by a beam stop. The shape of the intensity distribution of cylindrical objects is always the same even for very different materials, if the scattering angle is normalized to the "critical angle" θ_C of total reflection (see Fig. 2). This parameter depends only on the refractive index: $\theta_C^2 = 2\varepsilon$. The intensity of the deflected X-rays falls down to nearly zero at the critical angle of total reflection (see Fig. 2).
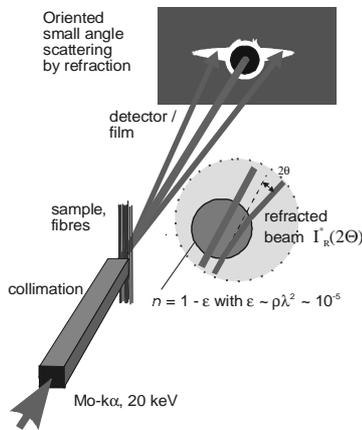

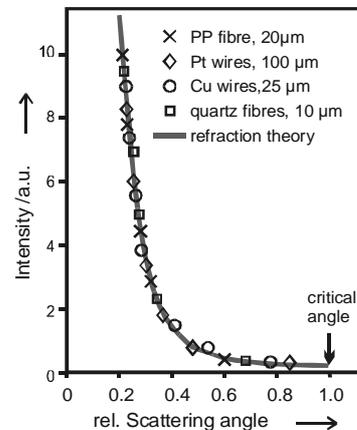**Figure 1:** Effect of oriented small angle scattering by refraction of glass fibers.

Figure 2: The normalized shape of the angular intensity distribution of cylindrical objects.

A cross section of 10^{-3} of the fiber diameter contributes to the detectable intensity above typically 2 minutes of arc. The effect of total reflection of X-rays occurs as well at the angle of grazing incidence but only 10^{-6} of the diameter is involved and therefore negligible. But well oriented planar surfaces can produce strong reflections. Based on Snell's Law the angular intensity distribution has been calculated and approximated for cylindrical fibers and spheres, as illustrated by Fig. 2. The refracted intensity of a cylinder without absorption effects can be expressed as in[2] equation 2.

$$I^*_R(2\theta') = \frac{J_0 \cdot 2R}{\varepsilon} \sin^3\left(\arctan\frac{\varepsilon}{\theta'}\right) = \frac{J_0 \cdot 2R \cdot \varepsilon^2}{\theta'^3} \qquad (2)$$

J_0 is the irradiation density of the incident X-ray beam onto the fiber, R is the radius of the fiber and $2\theta'=\theta$ is the scattering angle.

The SAXS instrumentation is relatively simple (see Fig. 3) but sometimes delicate in terms of its (thermo-) mechanical stability. It requires a collimated X-ray beam, a specimen manipulator, an X-ray refraction detector and a reference detector to monitor the specimen absorption and beam stability. The refraction intensity can be measured[3] according to equation 3.

$$I^*_R(2\theta') = I_R(2\theta') - I_{R0}(2\theta') \cdot \frac{I_A}{I_{A0}} = I_A \cdot k \cdot d \cdot N \cdot R \qquad (3)$$

I^*_R depends on the transmitted intensity I_A, the thickness d and the inner surface density $\Sigma = N \cdot R$ (N is the amount of fibers) of the specimen, respectively. The proportional factor k is a specific constant of the used apparatus and can be

determined by measuring a probe with a known inner surface density. The proportional factor k and the inner surface density Σ define the refraction value $C = k \cdot \Sigma$, which is a relative measure of the surface density of the specimen. For practical measurements the refraction detector remains at a fixed scattering angle $2\theta'$, so that the surface density of the specimen can be measured according to:

$$C = \frac{1}{d} \cdot \left(\frac{I_R \cdot I_{A0}}{I_{R0} \cdot I_A} - 1 \right)$$

(4)

The conventional understanding of "continuous" small angle X-ray scattering (SAXS) is governed by the interpretation of diffraction effects. Apart from Guinier's theory for separated particles Porod[4] explains diffraction of densely packed colloids similar to Eq. 3. However both deal with particles two orders of magnitude smaller.
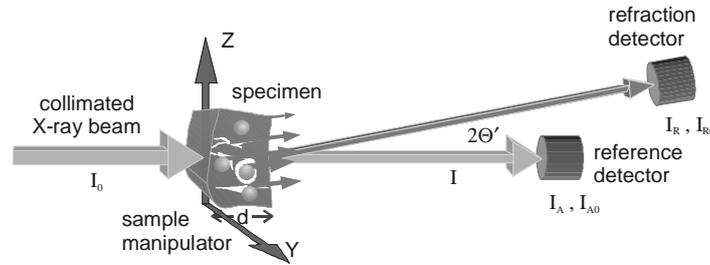

Figure 3: Basic principle of a SAXS instrumentation with collimated X-ray beam, specimen manipulator, a refraction detector, which measures the refracted intensity I_R of the specimen or I_{R0} if the specimen is not in place and a reference detector, which measures the intensity I_{A0} (without specimen) or I_A (with specimen), respectively.

A model composite has been made in order to demonstrate the refraction behavior of a bonded and debonded 140 μm sapphire fiber in a wax matrix (Fig. 4, left). The upper ray crosses the bonded fiber-matrix interface causing a small amount of deflected intensity. At the debonded fiber and at the matrix surfaces (lower ray) much more X-rays are deflected, as the larger density difference between the materials and air corresponds to a higher index of refraction.
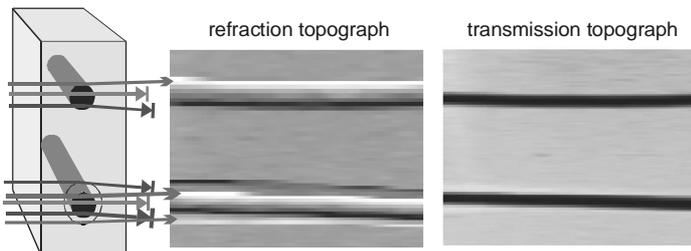

Figure 4: left; Model composite made of wax with a bonded (top) and debonded (bottom) 140 μm sapphire fiber. Middle; X-ray refraction at the interface of the bonded (top) and debonded (bottom) fiber. Right; X-ray transmission topograph of the model composite.
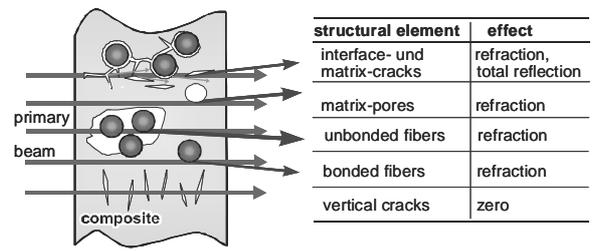
Figure 5: Sketch of various interfaces in a composite which causes X-ray refraction. The size of the refraction arrow indicates the strength of the measured refraction intensity.

The middle of Fig. 4 shows the resulting intensity distribution of a refraction scan of the model composite. The wax channel is clearly separated from the fiber surface. The bonded fiber is less contrasted. The right part of Fig. 4 shows the intensity distribution due to X-ray absorption of the model composite. In contrast to the refraction topograph a difference between the bonded (top) and debonded (bottom) fiber is not observably. Fig. 5 represents the various interfaces possible in a composite.

3   ANALYTICAL APPLICATIONS

Scanning X-ray refraction localizes the projection of inner surface concentrations or individual edges of surfaces and interfaces such as sub-micrometer pores or cracks. The spatial resolution can be better than 10 μm, although this is not the main advantage of refraction techniques, as the signal level itself contains the information about inner surfaces. Average specific surfaces can be determined by "stationary" X-ray refractometry. Such kind of analytical investigations can be useful in the field of new materials, when cutting or polishing has to be omitted. In Fig. 6 the specific surface

densities of selected non-metallic materials are compared. The values are relatively small in case of very "porous" materials as the pores are very large, which reduces the surface to volume ratio. The plotted surface values are taken from the refraction factors C, corrected for the different densities of the materials: C/ρ^2 (see Eqs. (1) and (2)). In case of composites like paper and carbon fiber reinforced plastics (CFRP) the refraction value C is a composition of the refraction at inner surfaces of each component and at the interfaces. In case of the CFRP the porosity is very low, therefore only the interface contributes to the signal. The measuring time is usually a few seconds or less, if ±1% error is accepted. The short measurement time allows scanning for spatial resolution or statistical evaluations.
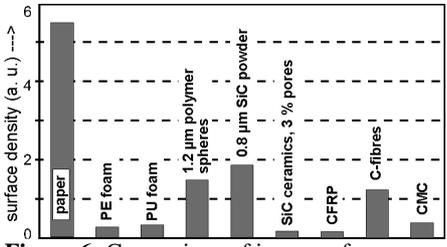

Figure 6: Comparison of inner surface densities of selected non-metallic materials
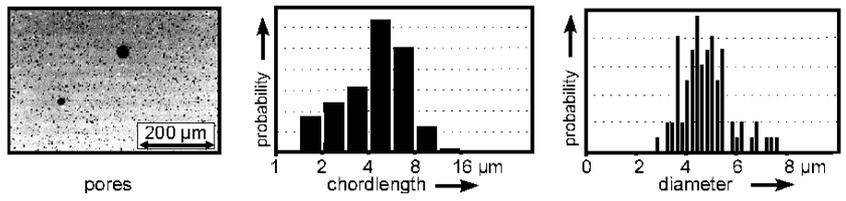
Figure 7: Pores in glass ceramics: micrograph, optical chord length analysis of pores and pore diameter probability by X-ray Refraction

The determination of the pore size distribution in glass ceramics by X-ray refraction results in diameters which correspond to the chord length distribution in microscopic analysis. The mean values of the diameters are identical within ±3%. The measurements are performed with Mo-k-α-radiation at different positions of a 1.4 mm ceramics plate, sintered at 850°C (Fig. 7). Further pore size measurements on SiC and Al_2O_3 ceramics by X-ray refractometry reveal good agreement with other techniques, especially with high pressure mercury intrusion.

3.1 Aging of aircraft composites
The measurement of the crack density in light weight materials can be performed by X-ray refractometry as well. The knowledge of the crack development is believed to play the key role in all long-term material behavior. Fig. 8 shows the results of an investigation which was made on matrix systems for high temperature applications in supersonic aviation.
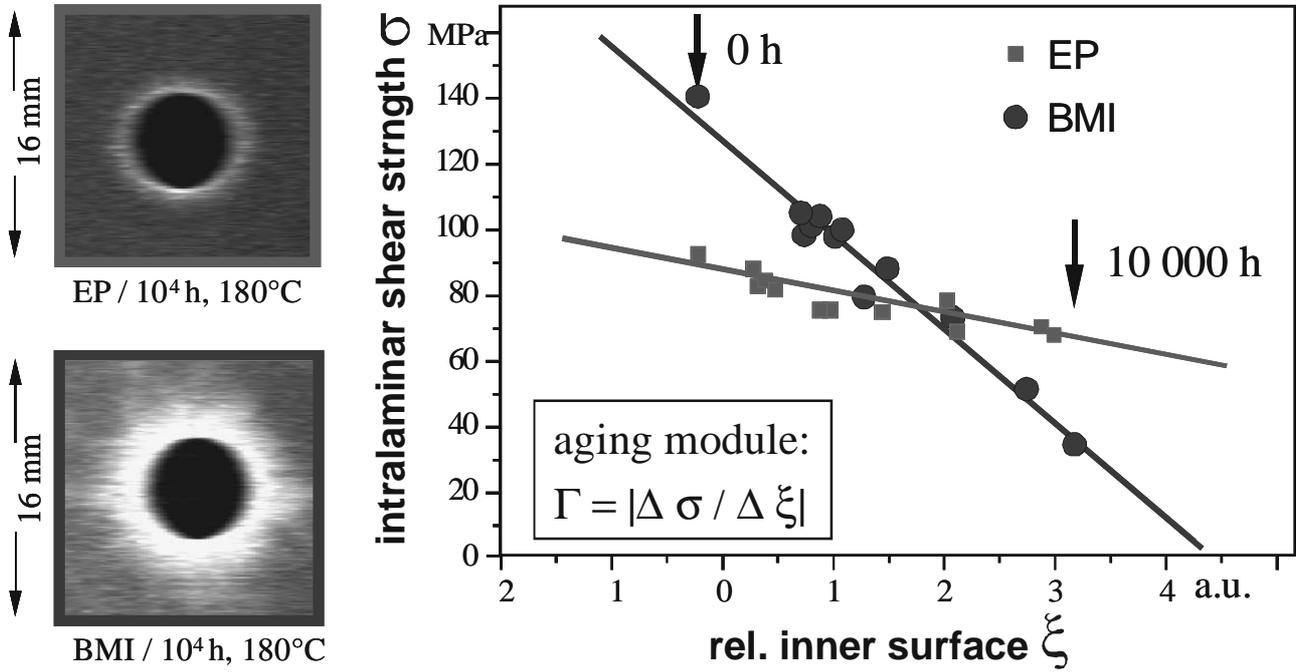

Figure 8: left, crack pattern in unidirectional CFRP after aging of 10,000 h at 180°C (top for EP, bottom for BMI). Right, Correlation of the residual shear strength of CFRP to the average inner surface of cracks created by aging treatment at 150 °C, 180 °C, 200 °C for 1000, 3000, 5000, 10000 h.

Fig. 8 top left shows a refraction topograph of a CFRP specimen made of an epoxy matrix system (EP) with a punched rivet hole in the center. The specimen was heat treated at 180 °C in a humid atmosphere for 10000 hours. Fig. 8 bottom left shows the refraction topograph for a specimen made of a bismaleine imide matrix system (BMI) and treated the same way as the specimen above. The bright area around the rivet hole indicates fiber matrix debonding (the brighter the intensity the stronger the damage). Thus the comparison of both topographs indicates a less tolerant behavior of the BMI system against the treatment compared to the EP system. Fig. 8 right shows for the investigated specimens the correlation between the residual intra laminar shear strength σ and the average inner surface ξ of cracks created by the aging treatment at 150°C, 180°C and 200°C for up to 10000 h. Although BMI has a high strength at the beginning, it falls below epoxy at the end of the aging treatment. The results explain clearly the dependence of the shear strength on the crack density. The slope defines an aging module which can be regarded as a new materials parameter[5].

3.2 Impact detection

Another problem of CFRP characterization relates to impact damages. Ultrasound C-scans resolve delaminations created by impact very well, but the single fibre debonding area, which develops at lower loads, is only detectable by X-ray refraction topography. Fig. 9 shows refraction topographs of a series of 0/90 CFRP laminates with different impact energies. The broadening and brightness of the refraction intensity is proportional to the damage in the composite. The total damage of the laminates is given by addition of 0 and 90 degrees fibre direction. The refraction values are plotted versus the absorbed energy per layer. In this case the correlation was linear.
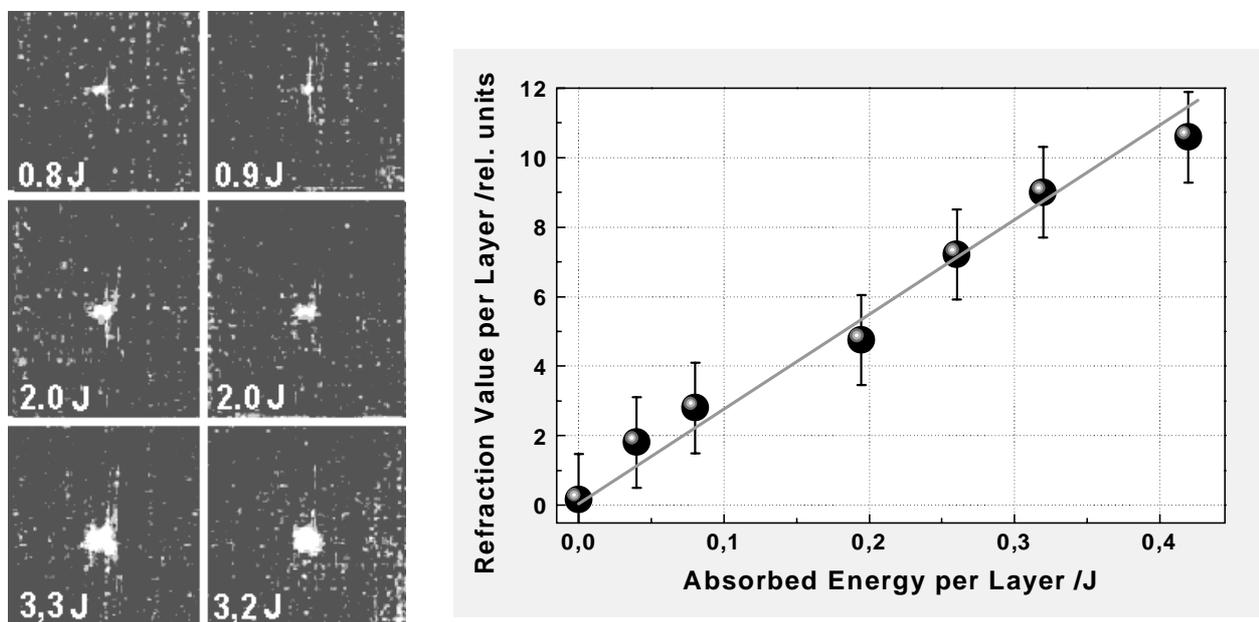

Figure 9: left, six 0/90 CFRP specimens with different impact energies. Right, linear correlation between the measured refraction values and the absorbed impact energy per layer in 0/90 CFRP laminates.

4   3D SYNCHROTRON REFRACTION COMPUTED TOMOGRAPHY

To enlarge the propulsive force of the next generation of aircraft engines some fundamental constructive changes has to be done. E.g. the design of the compressor section has to be changed from bladed disks (BLISK) to bladed rings (BLING) to archive a larger hub bore diameter for new compressor designs. This constructive changes (see Fig. 10 left) presuppose new materials which have the same stiffness at a lower weight. Fiber reinforced Titanium Metal Matrix Composites are especially suited to be used in the compressor part of an aircraft engine.

The cylindrical specimens for the test program have been provided by MTU Aero Engines. As reinforcing fiber the SCS6-fibre from Textron was taken. It has a 33 µm diameter carbon fiber as a core with a 1 µm pyro-C-protective

coating, followed by SiC and again by a pyro-C-protective coating of 3 µm (see Fig. 10, middle). The overall diameter of the fiber measures 140 µm.
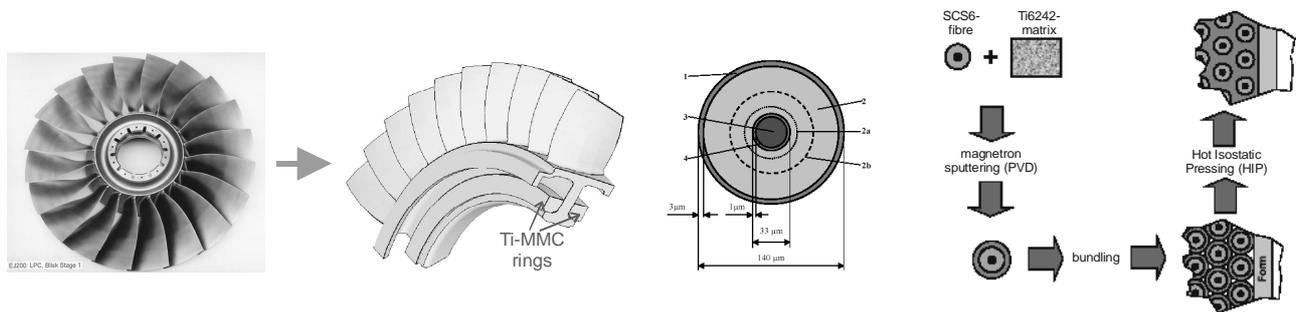

Figure 10: left, for a larger hub bore diameter for new compressor designs the Bladed disk BLISK has to be changed to Bladed ring BLING. Middle, Assembly of the SCS6-fibre from Textron (1: pyro-C-protective coating, 2: SiC, 3: C-fiber, 4: pyro-C-protective coating) and the HIP procedure of the Low Cycle Fatigue specimen manufacturing (right).

The fibers are coated (30 µm) with the titanium base alloy Ti6242 by magnetron sputtering and than bundled and formed by Hot Isostatic Pressing (HIP) (see Fig. 10, middle and right). Static and cyclic forces were applied parallel to the fibers which leads to the evaluation of the mechanical parameters. After the tests the specimens were examined by metallographic methods and the fractured surfaces were analyzed. As a new approach for non-destructive testing the specimens were investigated by 3D X-ray Refraction Computed Tomography at the materials research test station of BAM (BAMline) at the Synchrotron Facility in Berlin (BESSY) as well. The investigations should reveal whether the development of cracks and fiber failures after tensile load is distributed homogeneously across the sample, or locally concentrated.

4.1 Experimental set up for 3D Synchrotron Refraction Computed Tomography

In our laboratory we have employed conventional X-ray tubes, crystallographic small angle scattering cameras and scintillation counters, respectively. The specimens where scanned or rotated across a single beam under pre selected fixed scattering conditions in order to receive spatial resolution as described is section 3. However the measurements are relatively time consuming and due to low X-ray energies from characteristic radiation of Cu- and Mo-anodes restricted to low density materials. Most of these disadvantages have overcome by use of synchrotron radiation. At the Berliner Electron Storage Ring for Synchrotron Radiation (BESSY) the Federal Institute for Materials Research and testing (BAM) has build up a hard X-ray beamline[6] and an X-ray laboratory for materials research. The usable photon energy range of the beamline extends from 5 keV up to 60 keV for monochromatic radiation. The main advantages of Synchrotron Radiation are the high photon flux, the continuous energy range and the highly collimated and parallel photon beam, respectively. With the help of a monochromator system the appropriate photon energy can be chosen for the investigations. The experimental set up is sketched in Fig. 11. A parallel and monochromatic beam (up to 60 keV) with a band width of about 2% is delivered by the Double-Multilayer-Monochromator (DMM) of the beamline. For a good transparency of the specimen we used a 50 keV photon beam. The beam has a horizontal width of up to 30mm and a vertical width of a few millimeters, respectively. The beam from the DMM is than reflected by two Si(111) single crystals in a symmetric configuration. They are set to there Bragg condition for the chosen energy. An X-ray sensitive CCD-camera is placed behind the second crystal. It detects the photons reflected by the second crystal with a lateral resolution of about $5,3 \times 5,3 \ \mu m^2$. The Rocking curve width of the second crystal against the first crystal is FWHM=$3,9 \cdot 10^{-4}$ Degree (see Fig. 11, bottom right, open circles). Different from the set up for phase contrast CT, the sample is situated in the X-ray beam between the two crystals. The highly collimated and monochromatized beam from the first crystal transmits the specimen and will be attenuated according to the absorption properties of the specimen. Additionally, the beam is deflected due to the refraction effect at all interfaces in the composite as explained above. This leads to a broadening of the Rocking curve as shown in Fig. 11 (bottom right, filled circles) to FWHM=$4,9 \cdot 10^{-4}$ Degree.
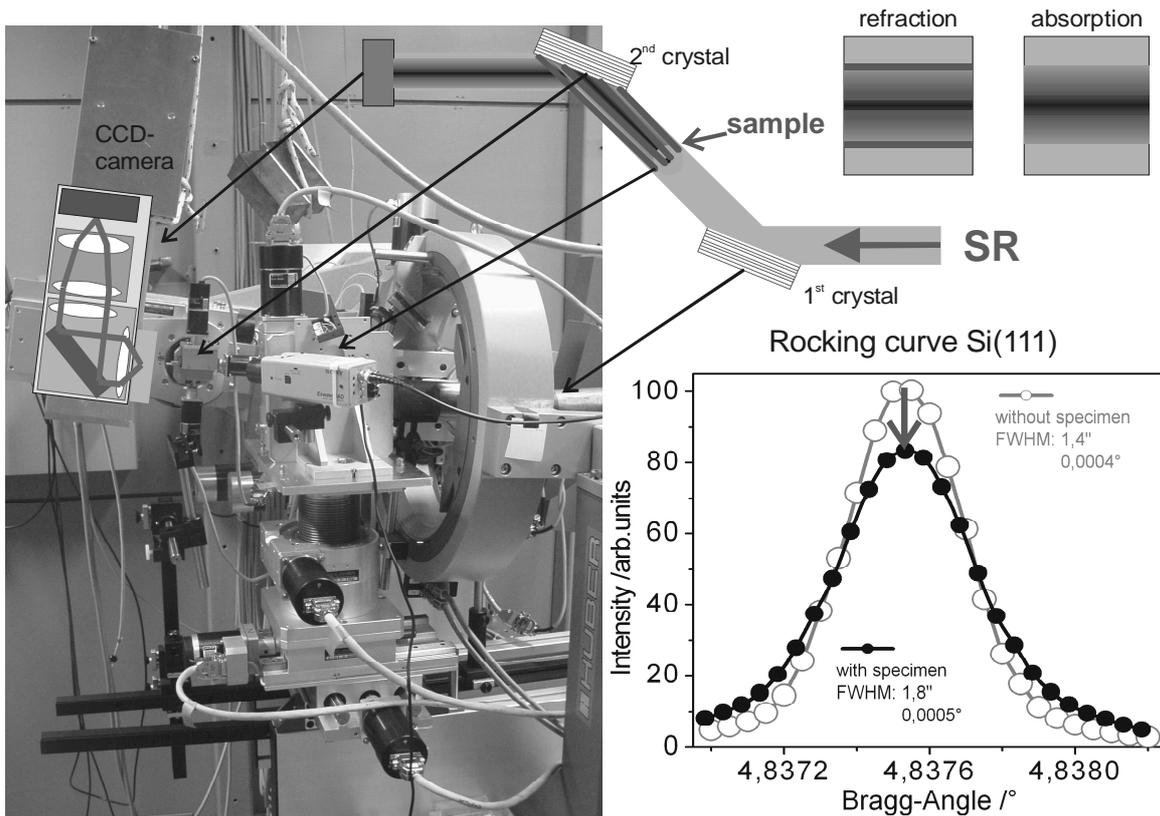
Figure 11: Sketch and photograph of the experimental set up at the BAMline. Bottom right: Rocking curve of the Si(111) single crystal pair in symmetric configuration from with specimen (filled dot) and without specimen (open circle) between the two crystals. The area under the curves is set to equal.

4.2 Measurements and results

Although two-dimensional refraction topography provides an effective new probe for analyzing meso-structures of all kind of heterogeneous materials, it is sometimes interesting to have section images of transversal resolution as known from X-ray computed tomography in order to overcome the overlap of details by projection effects. The measurements were performed by rotating the specimens around there cylindrical symmetry axis for 360 degrees in steps of 1 degree. After each step an exposure was taken. The data sets were analyzed by filtered back projection as known from the data treatments for conventional absorption CT.

Fig. 12 shows the reconstruction of one plane out of 300 planes of the absorption data set, which was taken in our CT-laboratory (100 kV, 4,7 x 4,7 x 4,7 μm^3 Voxel). It shows the cross section of a LCP specimen. The reinforcing SiC-fibers are shown up as dark discs with a slightly darker core. They are not symmetrically arranged to the rotational axis of the specimen. A crack (dark area) can be realized in the right part of Fig 10, which corresponds very well with the visible crack at the cladding of the specimen. No further indications can be seen for cracks or fiber failure in the remaining area.

Fig. 13 demonstrates the feasibility of X-ray refraction computed tomography performed at the BAM*line* at BESSY (50 keV, 5,3 x 5,3 x 5,3 μm^3 Voxel). It shows the same part of the specimen as Fig. 12 does, but even if the filtered back projection and the reconstruction is not jet adapted to the refraction effect, the information content is much higher. The absorption information is the same as in Fig. 12. But in addition the refraction effect reveal, that the crack distribution in the matrix (red colored areas) is much broader than expected from the absorption information.
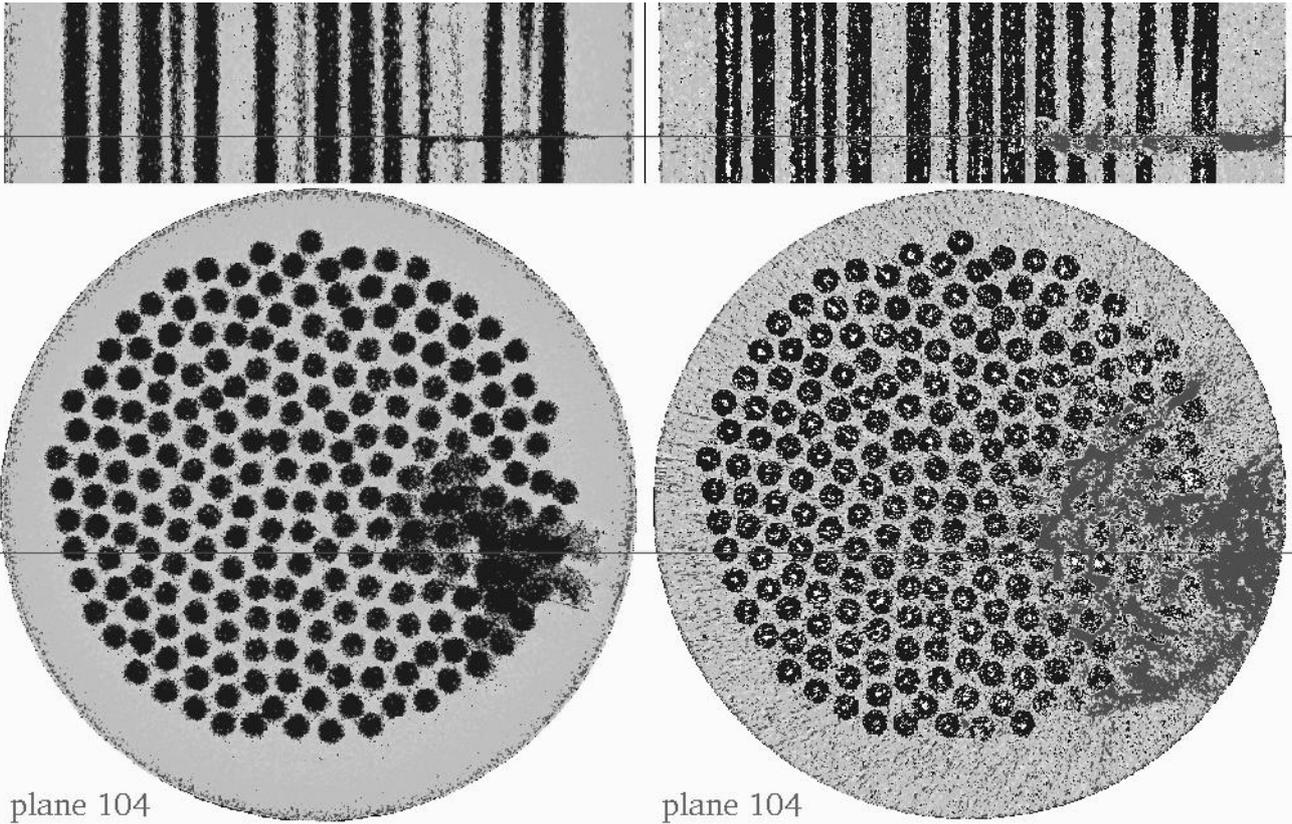
Figure 12: Reconstruction of the absorption measurement. 100 kV, 4,7 x 4,7 x 4,7 μm³ Voxel. Top, vertical cut through the specimen as indicated by the red line in the bottom.

Figure 13: Reconstruction of the refraction measurement. 50 keV, 5,3 x 5,3 x 5,3 μm³ Voxel. Specimen between two crystals. Top, vertical cut through the specimen as indicated by the red line in the bottom.

5   CONCLUSIONS

X-ray refraction techniques combine analytical capabilities of sub-micrometer structure detection with the requirements of non-destructive full volume characterization. Its potential of contrasting cracks and pores will be an alternative to other attempts on raising the spatial resolution of CT machines. X-ray refraction therefore might help faster materials development, better understanding of meso-structures and partly replace micro analysis and mechanical testing in advanced materials science.

REFERENCES

1. A. H. Compton, S.K. Allison, *X-ray in Theory and Experiment*, Macmillan and Co. Ltd., London, 1935.
2. M.P. Hentschel, R. Hosemann, A. Lange, B. Uther, R. Brückner, "Röntgenkleinwinkelbrechung an Metalldrähten, Glasfäden und hartelastischem Polypropylen", *Acta Cryst.*, **A 43**, 506-513, 1987.
3. M.P. Hentschel, K.-W. Harbich, A. Lange, "Nondestructive evaluation of single fibre debonding in composites by X-ray refraction", *NDT&E International*, **27**, 275-280, 1994.
4. G. Porod, "Die Röntgenkleinwinkelstreuung von dichtgepackten kolloidalen Systemen, I. Teil", *Kolloid.-Z.*, **124**, 83-114, 1951.
5. D. Ekenhorst, A. Lange, M.P. Hentschel, „Röntgen-Refraktion", *Materialprüfung*, **39**, 175-179, 1997.

6   W. Görner, M.P. Hentschel, B.R. Müller, H. Riesemeier, M. Krumray, G. Ulm, W. Diete, U. Klein, R. Frahm, "BAMline: the first hard X-ray beamline at BESSY II", *Nuclear Instruments and Methodes in Physics Researche*, **A467-468**, 703-706, 2001.